Science Translational Medicine AAAS

Cortical GABAergic excitation contributes to epileptic activities around human glioma

Johan Pallud *et al.*

Sci Transl Med **6**, 244ra89 (2014);
DOI: 10.1126/scitranslmed.3008065

Editor's Summary

Chloride Causes Seizures in Glioma

Gliomas, a common brain tumor, frequently induce epileptic seizures as they grow, but it is not clear why. Pallud *et al.* show that the epileptic activity in the brain around gliomas happens because neurons respond anomalously to the neurotransmitter GABA. Usually GABA turns neurons off, but when gliomas are nearby, it turns them on instead. Also seen in temporal lobe epilepsy, this unusual cell behavior happens because the neurons take up too many chloride ions. Glioma tumor cells also take up too much chloride, which helps them spread and invade into normal brain tissue. Perhaps drugs that block chloride uptake could interfere with both glioma-induced seizures and tumor growth, a two-for-one hit.

Science Translational Medicine (print ISSN 1946-6234; online ISSN 1946-6242) is published weekly, except the last week in December, by the American Association for the Advancement of Science, 1200 New York Avenue NW, Washington, DC 20005.

CANCER

Cortical GABAergic excitation contributes to epileptic activities around human glioma

Johan Pallud,[1,2,3,4] Michel Le Van Quyen,[1,2]* Franck Bielle,[1,5]* Christophe Pellegrino,[6,7]* Pascale Varlet,[4,8] Marianne Labussiere,[1,2] Noémie Cresto,[1,2] Marie-Joseph Dieme,[5] Michel Baulac,[1,2,9] Charles Duyckaerts,[1,5] Nazim Kourdougli,[6,7] Geneviève Chazal,[6,7] Bertrand Devaux,[3,4] Claudio Rivera,[6,7,10] Richard Miles,[1,2] Laurent Capelle,[1,11] Gilles Huberfeld[1,2,9,12,13]†

Brain gliomas are highly epileptogenic. Excitatory glutamatergic mechanisms are involved in the generation of epileptic activities in the neocortex surrounding gliomas. However, chloride homeostasis is known to be perturbed in glioma cells. Thus, the contribution of γ-aminobutyric acidergic (GABAergic) mechanisms that depend on intracellular chloride merits closer study. We studied the occurrence, networks, cells, and signaling basis of epileptic activities in neocortical slices from the peritumoral surgical margin resected around human brain gliomas. Postoperative glioma tissue from 69% of patients spontaneously generated interictal-like discharges, synchronized, with a high-frequency oscillation signature, in superficial layers of neocortex around areas of glioma infiltration. Interictal-like events depended both on glutamatergic AMPA receptor–mediated transmission and on depolarizing GABAergic signaling. GABA released by interneurons depolarized 65% of pyramidal cells, in which chloride homeostasis was perturbed because of changes in expression of neuronal chloride cotransporters: KCC2 (K-Cl cotransporter 2) was reduced by 42% and expression of NKCC1 (Na-K-2Cl cotransporter 1) increased by 144%. Ictal-like activities were initiated by convulsant stimuli exclusively in these epileptogenic areas. This study shows that epileptic activities are sustained by excitatory effects of GABA in human peritumoral neocortex, as reported in temporal lobe epilepsies, suggesting that both glutamate and GABA signaling and cellular chloride regulation processes, all also involved in oncogenesis as already shown, induce an imbalance between synaptic excitation and inhibition underlying epileptic discharges in glioma patients. Thus, the control of chloride in neurons and glioma cells may provide a therapeutic target for patients with epileptogenic gliomas.

INTRODUCTION

Diffusely growing gliomas, graded as grades II to IV according to World Health Organization (WHO) definition, are highly epileptogenic primary brain tumors in adults. Epilepsy incidence varies from 60 to 100% in low-grade and 25 to 60% in high-grade gliomas (*1*, *2*). Epileptic activities seem to arise from the neocortex surrounding gliomas (*3*–*5*), and glioma cell infiltration may promote growth and recurrence of tumors at sites around their spatial core (*6*, *7*).

Epileptic activity has often been linked to changes in the balance between excitatory and inhibitory synaptic signaling. Recent data show that massive excitatory glutamate release (*8*) underlies epileptic activity and contributes to neuronal death as tumors progress. Potassium (K^+) buffering (*9*, *10*) and glutamate clearance (*11*–*13*) are both impaired so that extracellular levels are elevated in peritumoral neocortex (*14*–*17*).

[1]Sorbonne Universités, University Pierre and Marie Curie (UPMC) University of Paris 06, F-75005 Paris, France. [2]Institut du Cerveau et de la Moelle Epinière, INSERM UMRS975, CNRS UMR7225, UPMC University of Paris 06, F-75013 Paris, France. [3]Service de Neurochirurgie, Centre Hospitalier Sainte-Anne, F-75014 Paris, France. [4]University Paris Descartes, Pôle de recherche et d'enseignement supérieur (PRES) Sorbonne Paris Cité, F-75005 Paris, France. [5]Service de Neuropathologie, Centre Hospitalo-Universitaire Pitié-Salpêtrière, Assistance Publique–Hôpitaux de Paris (AP-HP), F-75013 Paris, France. [6]INSERM, Institut de Neurobiologie de la Méditerranée (INMED), Parc Scientifique de Luminy, F-13009 Marseille, France. [7]Aix-Marseille University, UMR S901, Parc Scientifique de Luminy, F-13009 Marseille, France. [8]Service de Neuropathologie, Centre Hospitalier Sainte-Anne, F-75014 Paris, France. [9]Unité d'Epileptologie, Centre Hospitalo-Universitaire Pitié-Salpêtrière, AP-HP, F-75013 Paris, France. [10]Neuroscience Center, University of Helsinki, 00014 Helsinki, Finland. [11]Service de Neurochirurgie, Centre Hospitalo-Universitaire Pitié-Salpêtrière, AP-HP, F-75013 Paris, France. [12]Département de Neurophysiologie, UPMC, Centre Hospitalo-Universitaire Pitié-Salpêtrière, AP-HP, F-75013 Paris, France. [13]Infantile Epilepsies and Brain Plasticity, INSERM, Unit U1129, University Paris Descartes, PRES Sorbonne Paris Cité, CEA, F-75015 Paris, France.
*These authors contributed equally to this work.
†Corresponding author. E-mail: gilles.huberfeld@upmc.fr

On the other hand, neuronal inhibition may be defective. In the neocortex surrounding a tumor, γ-aminobutyric acid A ($GABA_A$) receptor expression (*18*) and the numbers of inhibitory interneurons and synapses are reduced (*5*, *19*, *20*). Work on nontumoral human epileptic tissue suggests that GABAergic synapses generate depolarizing effects, which contribute to epileptic activities (*21*–*24*). $GABA_A$ receptor channels are mainly permeable to chloride (Cl^-). If the driving force for Cl^- induces an inward Cl^- flux, a cell will be hyperpolarized. In contrast, an outward flux of Cl^- will depolarize neurons and may result in a functional excitation. In mature neurons, intracellular Cl^- concentration is normally maintained at low levels, by extrusion via the K-Cl cotransporter 2 (KCC2), whereas Cl^- loading by Na-K-2Cl cotransporter 1 (NKCC1) is reduced (*25*). Recent data on human tissue suggest that Cl^- homeostasis is altered in gliomas. Cl^- concentrations are increased both in neurons (*26*, *27*) and in migrating glioma cells (*28*, *29*), loaded by NKCC1 (*26*, *30*, *31*), which is highly expressed in human peritumoral neocortex (*32*). The loading of neurons with Cl^- may underlie epileptogenic effects, whereas its accumulation in glioma cells contributes to oncologic processes. We therefore asked whether the effects of a defective Cl^- homeostasis on GABAergic signaling might be involved in epileptogenesis in human peritumoral neocortex.

RESULTS

Identification of a spontaneous interictal-like activity

We studied 81 slices from 47 fresh brain tissue specimens obtained from the "surgical margin" (the removed neocortex that surrounds the macroscopic tumor) from 29 patients with supratentorial, hemispheric, and diffuse low-grade (n = 17, WHO grade II) or high-grade (n = 12, 4

WHO grade III and 8 WHO grade IV) gliomas (Fig. 1A and table S1) (*33*). Spontaneous activity was recorded from 74 of 81 (91.4%) slices from 42 of 47 (89.4%) brain tissue specimens from 28 of 29 (96.6%) patients. The activity included spontaneous interictal-like discharges (IIDs), consisting of a field potential and multiunit firing, in records from 36 of 81 slices (44.4%) from 25 of 47 tissues (53.2%) from 20 of 29 patients (69%) (Fig. 1B). Multiunit discharges alone were recorded from the remaining 38 of 45 slices (84.4%). IIDs were more frequent in slices (n = 32 of 66, 48.5%) from patients (n = 17 of 22, 77.3%) with preoperative seizures than in those (n = 4 of 15, 26.7%) from patients (n = 3 of 7, 42.9%) without seizures (P = 0.05) (Fig. 1C).

Spatial distribution of interictal-like activity

We asked whether sites of IID generation were correlated with regions of tumor infiltration. Only infrequent multiunit activity was recorded from tissue (14 slices from 7 patients) obtained at distances of

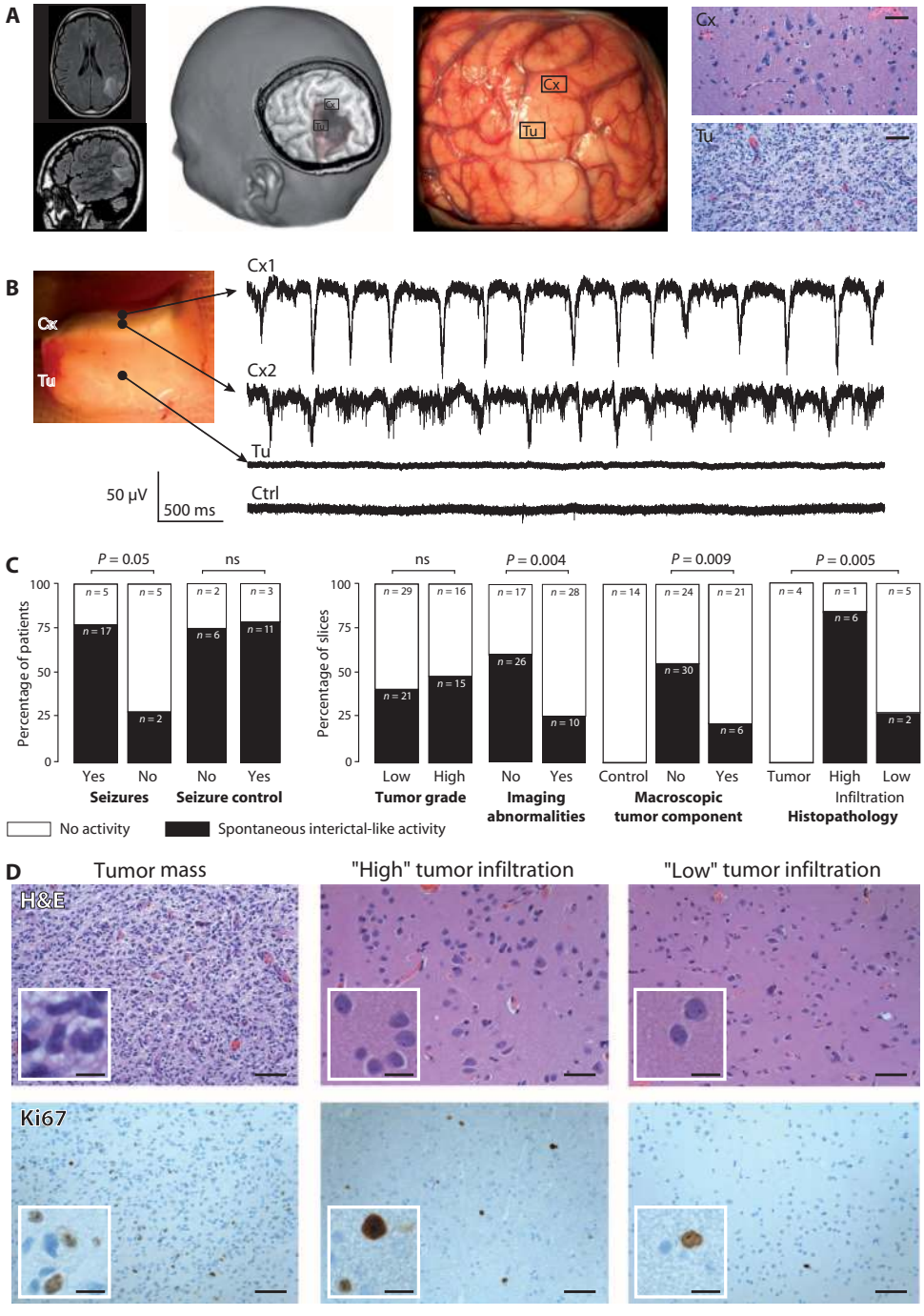

Fig. 1. IIDs are generated in the human neocortex infiltrated by glioma cells. (**A**) Example of a left parietal low-grade (WHO grade II) glioma. The tumor appears as a hypersignal area on a Fluid Attenuated Inversion Recovery (FLAIR) sequence (far left), as a hyposignal area on a three-dimensional spoiled gradient sequence (near left), and as pale, hypertrophied, and infiltrated gyri on intraoperative photographs (mid right). Brain tissue specimens were sampled inside the tumor (Tu) and from the neocortex (Cx) outside macroscopic tumor infiltration. In areas outside visible tumor abnormalities (Cx), we detected only an infiltration by glioma cells [hematoxylin and eosin (H&E) staining, ×200]. Tumor infiltration was obvious in tissue from areas of visible imaging tumor abnormalities (Tu; H&E staining, ×200). Scale bar, 100 µm. (**B**) Multiple extracellular recordings of IIDs from a slice containing both the solid tumor component and adjacent infiltrated neocortex. Electrode locations: Cx1, superficial neocortical layer; Cx2, mid-neocortical layers; Tu, solid tumor tissue. Ctrl shows a record from noninfiltrated neocortex in a control tissue from another tumor specimen. (**C**) The proportion of patients or slices from which IIDs were (black) or were not (white) detected, grouped by history of seizures (29 patients; P = 0.05, Fisher's exact test), preoperative seizure control with antiepileptic drugs [22 patients; ns, not significant (Fisher's exact test)], tumor grade (81 slices; low-grade versus high-grade; ns, Fisher's exact test), macroscopic tumor component on MRI (81 slices; inside versus outside regions of FLAIR hypersignal on MRI; P = 0.004, Fisher's exact test), presence of a macroscopic tumor component on gross histopathological analysis (81 slices; presence versus absence versus control; 14 slices; P = 0.009, Fisher's exact test), and histopathological analyses (18 slices; tumor mass versus high tumor infiltration versus low tumor infiltration by isolated tumor cells; P = 0.005, Fisher's exact test). (**D**) Classical histopathogical features of a glioma with H&E (upper) and Ki67 (lower) stains. The tumor mass (left) is devoted of any neurons. The area of high tumor infiltration (middle) is a neocortical tissue infiltrated by 10 or more tumor cells per high-power field. The area of low tumor infiltration (right) is a neocortical tissue infiltrated by isolated glioma cells (fewer than 10 glioma cells per high-power field). Scale bars, 100 µm; 25 µm (insets).

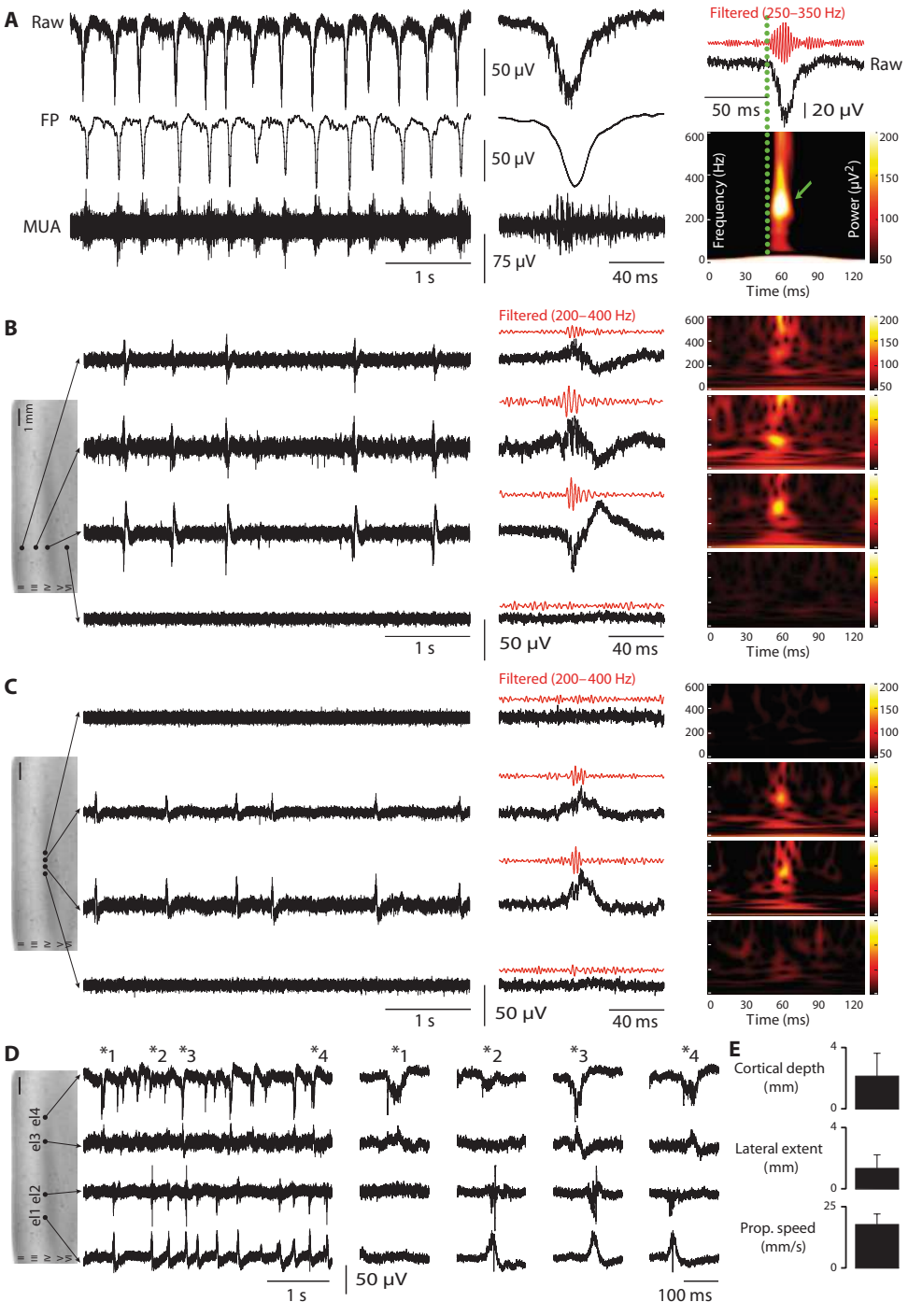

Fig. 2. IIDs are restricted to superficial neocortical layers and are generated in multiple sites. (**A**) Extracellular records of IIDs. They consist of bursts of multiunit activity (MUA; >300-Hz high-pass filter) correlated with field potentials (FP; <100-Hz low-pass filter) (left). Expanded raw, MUA, and FP traces are shown in the middle. HFOs (filtered to pass 250 to 350 Hz) are detected during IIDs (upper right). The green dotted line shows the onset of the IID FP. Time frequency plots (lower right) show a mean dominant frequency of 251 ± 69 Hz (n = 572 events). (**B** and **C**) Multiple extracellular records of IIDs from slices containing infiltrated neocortex. In (B), four electrodes are placed at different depths of the same neocortical column. They show that IIDs and HFOs were synchronous in a vertical column-like region with field onset, maximal amplitude, and the largest HFO at the deep border of layer III. In (C), four electrodes are placed at the interface between layers III and IV at the same depth over a lateral distance of 1 mm. They show a spatially restricted lateral spread of IIDs and HFOs. HFOs were never detected in the absence of IIDs. (**D**) IIDs are initiated at multiple foci in infiltrated neocortex. Multiple records from a slice of infiltrated neocortex with four electrodes (el) located at the interface between layers III and IV at separations of: el1—1 mm—el2—3 mm—el3—1 mm—el4. Expanded traces of events *1, *2, *3, and *4 are shown in the middle. (**E**) Mean ± SD of the neocortical depth, lateral extent, and propagation speed of IIDs in the recorded slices. IIDs were recorded at a mean maximal depth of 2.1 ± 1.5 mm (range, 0.5 to 5; n = 31 slices) from the pia mater, propagated laterally over a mean distance of 1.3 ± 0.94 mm (range 1 to 5; n = 22 slices) at a speed of 19 ± 3 mm s^{-1}.

~30 mm from image-defined abnormalities during surgical access to different tumors (Fig. 1B). Histopathological analysis revealed no tumor infiltration by isolated tumor cells at this distance in tissues obtained from these patients (7 slices from 4 insular gliomas, 4 slices from 2 frontal gliomas, and 3 slices from a mesial temporal glioma) (Fig. 1, B and C). IIDs were generated significantly more frequently in slices devoid of any macroscopic tumor component as defined on magnetic resonance imaging (MRI) and according to intraoperative localization ["outside imaging abnormalities" (60.5%) versus "inside" (26.3%); P = 0.004] and on histopathological analyses ["absence of macroscopic tumor component" (55.6%) versus "presence" (22.2%); P = 0.009] (Fig. 1C). IIDs were recorded more frequently in slices with high tumor infiltration (6 of 7, 85.7%) than in slices with low tumor infiltration (2 of 7, 28.7%) and never in slices with a solid tumor mass (0 of 4, 0%) (P = 0.005) (Fig. 1, C and D). A link between molecular defects in the glioma and the recording of IID was explored. The density of $CD3^+$ (P = 0.852), $CD20^+$ (P = 0.472), and $CD68^+$ cells (P = 0.645) and $Ki67^+$ cells in neocortex (P = 0.852) or in white matter (P = 0.772) had no significant influence (fig. S1).

Thus, IIDs are not generated in the tumor mass, but our recordings suggest that they may arise from regions of tumor infiltration surrounding neocortical gliomas.

Cortical organization and electrophysiological characteristics

IIDs consisted of field potential associated with bursts of multiunit firing (Fig. 2A). Their mean amplitude was 57.9 ± 11.5 μV (range, 22.5 to 166.2), their mean duration from onset to peak was 24.4 ± 7.9 ms (range, 7.4 to 44), and they recurred with a mean frequency of 0.9 ± 0.7 Hz (range, 0.1 to 4.2) (n = 9723 events; n = 36 slices). High-frequency oscillations (HFOs) were nested within IIDs in 40.7% of extracellular records (11 of 27 slices; n = 9 patients). They occurred during 71.9% of IIDs, and the mean dominant frequency was 251 ± 69 Hz (range, 150 to 350) (Fig. 2A). HFO were never recorded from control tissue or sites without IIDs (Fig. 2, B and C). HFOs thus tended to confirm the epileptic nature of IIDs (*34*).

IIDs were synchronous within "vertical" column-like regions in 31 of 36 slices (Fig. 2B). They were recorded at a mean maximal depth of 2.1 ± 1.5 mm (range, 0.5 to 5; n = 31 slices) from the pia mater (Fig. 2B). IIDs were initiated preferentially from layers III and IV (28 of 31 slices) and typically propagated to superficial layers (Fig. 2, C and D). HFOs were restricted to layers III and IV, suggesting that IIDs were generated locally. IIDs propagated from their initiation site over a mean lateral distance of 1.3 ± 0.94 mm (range, 1 to 5; n = 22 slices) (Fig. 2, C and E) at a speed of 19 ± 3 mm s^{-1}. Multiple, partly overlapping, asynchronous IID foci were detected in 25 of 36 slices (Fig. 2D). The mean distance between foci was 1.8 ± 1.2 mm (range, 0.7 to 5; n = 22 slices). Spatial patterns of IID initiation and spread were similar in adjacent slices from 10 of 30 brain tissue specimens.

Thus, IIDs are generated at multiple neocortical sites surrounding gliomas and are spatially restricted to superficial and mid-neocortical layers.

Pharmacology and cellular basis of interictal-like activity

We next examined the role of glutamatergic and GABAergic signaling in the genesis of IIDs. The *N*-methyl-D-aspartate

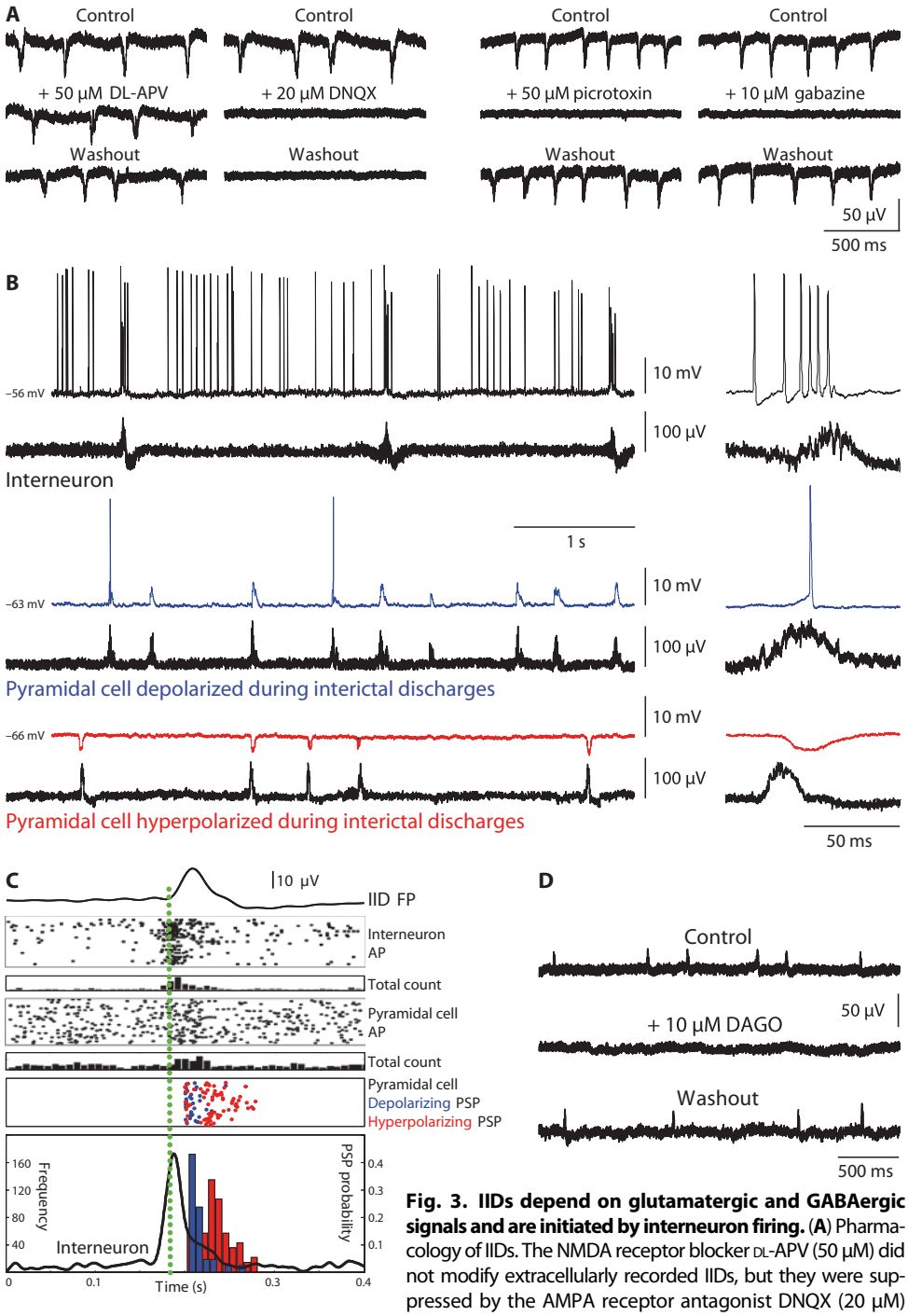

Fig. 3. IIDs depend on glutamatergic and GABAergic signals and are initiated by interneuron firing. (**A**) Pharmacology of IIDs. The NMDA receptor blocker DL-APV (50 μM) did not modify extracellularly recorded IIDs, but they were suppressed by the AMPA receptor antagonist DNQX (20 μM) (left). The $GABA_A$ receptor antagonists picrotoxin (50 μM) and gabazine (10 μM) reversibly blocked IIDs (right). (**B**) Cellular basis of IIDs. Spontaneous intracellular (upper) and extracellular (lower) records of neurons from infiltrated neocortex. Expanded traces of single IIDs at right. An interneuron (top, black) fired before and during IID initiation. Some pyramidal cells were depolarized (middle, blue), and others were hyperpolarized during IIDs (bottom, red). (**C**) Timing of cellular firing during IIDs. Mean population field activity (IID FP; top) plotted against sequential raster traces and peri-event histogram of interneuron firing (interneuron AP and count). Raster traces and peri-event histogram for firing of an excited pyramidal cell (pyramidal cell AP and count). The green dotted line shows the onset of the IID FP. Timing of the peak of depolarizing PSPs is shown by blue dots, and timing of the peak of hyperpolarizing PSPs is shown by red dots. The time course of interneuron firing (black line) and the probability of depolarizing (red) and hyperpolarizing PSPs (blue) are shown in the lower box. (**D**) Hyperpolarizing interneurons with DAGO (10 μM), a μ-opioid receptor agonist, reversibly suppressed IID FPs.

(NMDA) receptor antagonist DL-2-amino-5-phosphonopentanoic acid (DL-APV, 50 μM; $n = 6$) had no effect, but the AMPA receptor antagonist 6,7-dinitroquinoxaline-2,3-dione (DNQX, 20 μM; $n = 6$) irreversibly suppressed IIDs (Fig. 3A, left). IIDs were reversibly suppressed by $GABA_A$ receptor antagonists picrotoxin (50 μM; $n = 6$) or gabazine (10 μM; $n = 5$) (Fig. 3A, right). These data indicate that both excitatory and inhibitory synapses are involved in IID generation.

Intracellular recordings were made from single pyramidal cells and interneurons to characterize the neuronal and synaptic local network basis of IID generation and specifically to examine the role of depolarizing responses to GABA. The mean resting potential of recorded pyramidal cells [$n = 20$ from 11 epileptic patients (10 cells from grade II, 5 cells from grade III, and 5 cells from grade IV gliomas)] was −60.3 ± 8.1 mV (range, −50.0 to −79.0), and mean input resistance was 44.2 ± 15.8 MΩ (range, 30 to 68). Interneurons [$n = 2$, from 2 epileptic patients (1 grade II and 1 grade IV gliomas)] were distinguished by a fast firing pattern and a short action potential duration (*35*). They fired for 39 ± 7 ms (range, 22 to 199) before IID initiation at a mean frequency of 78 ± 36 Hz (range, 34 to 142; $n = 32$ events) and were always active during IIDs (Fig. 3B). The behavior of pyramidal cells during IIDs was variable. Cells distant from foci ($n = 3$ from 1 epileptic patient with a grade II glioma) did not consistently receive synaptic events during IIDs. Seventeen cells were recorded within the IID area. At resting potential, 6 (35.3%) of these neurons received hyperpolarizing synaptic events during IIDs (Fig. 3B). The remaining 11 of 17 cells (64.7%) received depolarizing synaptic events and sometimes fired during IIDs (Fig. 3B). In contrast to interneurons, they never discharged before the onset of the IID field. The resting membrane potential (mean, −62.6 ± 10.3 mV; range, −79.0 to −50.0) and the input resistance (mean, 47.0 ± 19.1 MΩ; range, 30.0 to 68.0) of cells that displayed depolarizing synaptic events were similar to the resting membrane potential (mean, −58.8 ± 4.6 mV; range, −68.0 to −56.0) and input resistance (mean, 40.1 ± 14.1 MΩ; range, 30.0 to 50.0) of cells that received hyperpolarizing synaptic events during IIDs ($P = 0.859$ and $P = 0.800$, respectively). The excitability of the two cell groups was also similar. Depolarizing pulses of 0.5 nA and duration of 100 ms induced action potentials at 6.9 ± 9.0 Hz in 11 cells that fired during IIDs, and identical stimuli applied to neurons that did not fire during IIDs induced action potentials at 6.8 ± 9.2 Hz ($P = 0.460$). We next compared the timing of firing and synaptic events received by interneurons ($n = 2$) and pyramidal cells ($n = 5$) during IIDs (Fig. 3C). Both interneurons consistently fired before IID onset and before pyramidal cell discharges. Depolarizing postsynaptic potentials (PSPs) also tended to precede hyperpolarizing PSPs, suggesting that interneuron firing may have contributed to IID initiation. We tested this hypothesis using the μ-opioid receptor agonist [3H][D-Ala^2,N-Me-Phe^4,Gly^5-ol] enkephalin (DAGO, 10 μM; $n = 5$) to hyperpolarize interneurons and effectively remove them from the local network. DAGO reversibly suppressed IIDs in all 5 of 5 cases (Fig. 3D), reinforcing the interneurons' drive hypothesis.

Depolarizing responses to GABA during IIDs

Interneuron firing preceded IID onset, and 64.7% of pyramidal cells were depolarized during IIDs. We asked whether pyramidal cell depolarization could result from $GABA_A$ release by measuring the compound reversal potential of PSPs impinging on pyramidal cells, which combine inhibitory and excitatory inputs [$n = 15$ from 9 epileptic patients (7 cells from grade II, 5 cells from grade III, and 3 cells from grade IV gliomas)] during IIDs (Fig. 4A). Two distinct behaviors were apparent (Fig. 4B). In 6 of 15 pyramidal cells (40%), synaptic events reversed negative to resting potential with a mean driving force of 7.8 ± 3.9 mV (range, 4 to 14) [mean reversal potential, −66.6 ± 4.0 mV (range, −72 to −62.5)]. In the remaining 9 of 15 cells (60%), synaptic events reversed at values depolarized from resting potential with a mean driving force of −13.4 ± 10.4 mV (range, −28 to −6) [mean reversal potential, −49.1 ± 10.8 mV (range, −40 to −73)]. The mean resting potential of the depolarized (−58.8 ± 4.6 mV; $n = 6$) and hyperpolarized (62.5 ± 10.0 mV; $n = 9$) subgroups of cells was not significantly different ($P = 0.414$). Thus, GABAergic signaling depolarized about 60% of pyramidal cells situated in IID foci, similar to the 65% of cells receiving a depolarizing PSP during IIDs.

Because IIDs were associated with depolarizing actions of GABA and were present in regions of tumoral infiltration, we asked whether the depolarizing effects of GABA were limited to zones of infiltration. In infiltrated tissues, 7 of 8 recorded pyramidal cells (87.5%) were depolarized by GABA during IIDs. In contrast, depolarization was detected in 4 of 9 cells recorded (44.4%) from tissue with no macroscopic or histopathological evidence for infiltration ($P = 0.050$) (Fig. 4B). The proportion of cells depolarized by GABA was higher in grade IV gliomas ($n = 5$ of 5) than in grade III ($n = 2$ of 5) or grade II ($n = 4$ of 7) gliomas ($P = 0.050$) (*33*).

Changes in expression or function of molecules that regulate Cl^- homeostasis could account for depolarizing GABAergic effects and contribute to tumor infiltration. The K-Cl cotransporter NKCC1 is expressed at low levels in nonjuvenile tissue (*36*), and Cl^- extrusion by the transporter KCC2 maintains low levels of internal Cl^- in mature tissues, assuring hyperpolarizing effects of GABA (*37*). We measured the levels of both transporters in Western blot analyses of 27 brain tissue specimens obtained from the "surgical margin" of 14 patients with supratentorial gliomas (6 grade II, 5 grade III, and 3 grade IV; 9 with a history of seizures) and from 4 patients with a cerebral metastasis of a carcinoma (4 control samples obtained during surgical access to deep-seated tumor; no history of seizures). NKCC1 protein expression was significantly increased in Western blots of peritumoral tissue (144 ± 31%) compared to control (100 ± 16%; $P = 0.004$) and was significantly increased in Western blot of tissues from epileptic patients (146 ± 31%) compared to nonepileptic patients (113 ± 25%; $P = 0.002$) (Fig. 4D). NKCC1 expression by glioma cells (*30*, *31*, *38*) might mask possible changes of the protein in neurons of the infiltrated neocortex. We therefore correlated NKCC1 expression with glioma infiltration. There was no significant difference of NKCC1 expression in peritumoral tissues with a high tumor infiltration (139 ± 25%) and those with a low tumor infiltration (146 ± 34%) using a neuron-specific reference protein (β3-tubulin; $P = 0.676$) or using a glial-specific reference protein (α-tubulin; 192 ± 52% versus 158 ± 65%; $P = 0.833$) (fig. S2). Similarly, there was no significant difference of NKCC1 expression between high-grade gliomas (139 ± 25%) and low-grade gliomas (146 ± 35%; $P = 0.676$). An up-regulation of NKCC1 in peritumoral pyramidal cells seems likely to have epileptogenic actions. We tested this hypothesis using bumetanide at doses that act selectively to suppress NKCC1 function in neurons (8 μM). In 6 of 6 slices, bumetanide reversibly suppressed IIDs over a period of 50 ± 10 min (range, 45 to 60), presumably reflecting the time taken to establish new steady-state Cl^- levels in neurons (Fig. 4C). These results reflect an increase in chloride loading, highlighting a possible change in chloride flux after $GABA_A$ receptor activation.

Because intraneuronal concentrations of Cl^- mainly depend on equilibrium between NKCC1-mediated Cl^- load and KCC2-mediated

Cl^- extrusion, we then investigated KCC2 protein expression. KCC2 protein was significantly decreased in Western blot of peritumoral tissue (42 ± 36%) compared to control (100 ± 44%; $P = 0.031$). Nevertheless, KCC2 was not significantly decreased in Western blot of tissues from epileptic patients (40 ± 35%) compared to nonepileptic patients (75 ± 49%; $P = 0.158$) (Fig. 4C). There was also no significant difference of KCC2 expression in peritumoral tissues with high tumor infiltration (43 ± 37%) and those with low tumor infiltration (39 ± 39%; $P = 0.112$). Similarly, there was no significant difference of KCC2 expression in high-grade gliomas (44 ± 37%) and low-grade gliomas (41 ± 38%; $P = 0.899$). Because protein expression does not demonstrate function of the protein, we next examined neuronal expression of KCC2 by immunohistochemistry with a KCC2-specific antibody (Fig. 4E). The number of KCC2 negative neurons was significantly higher in peritumoral tissue

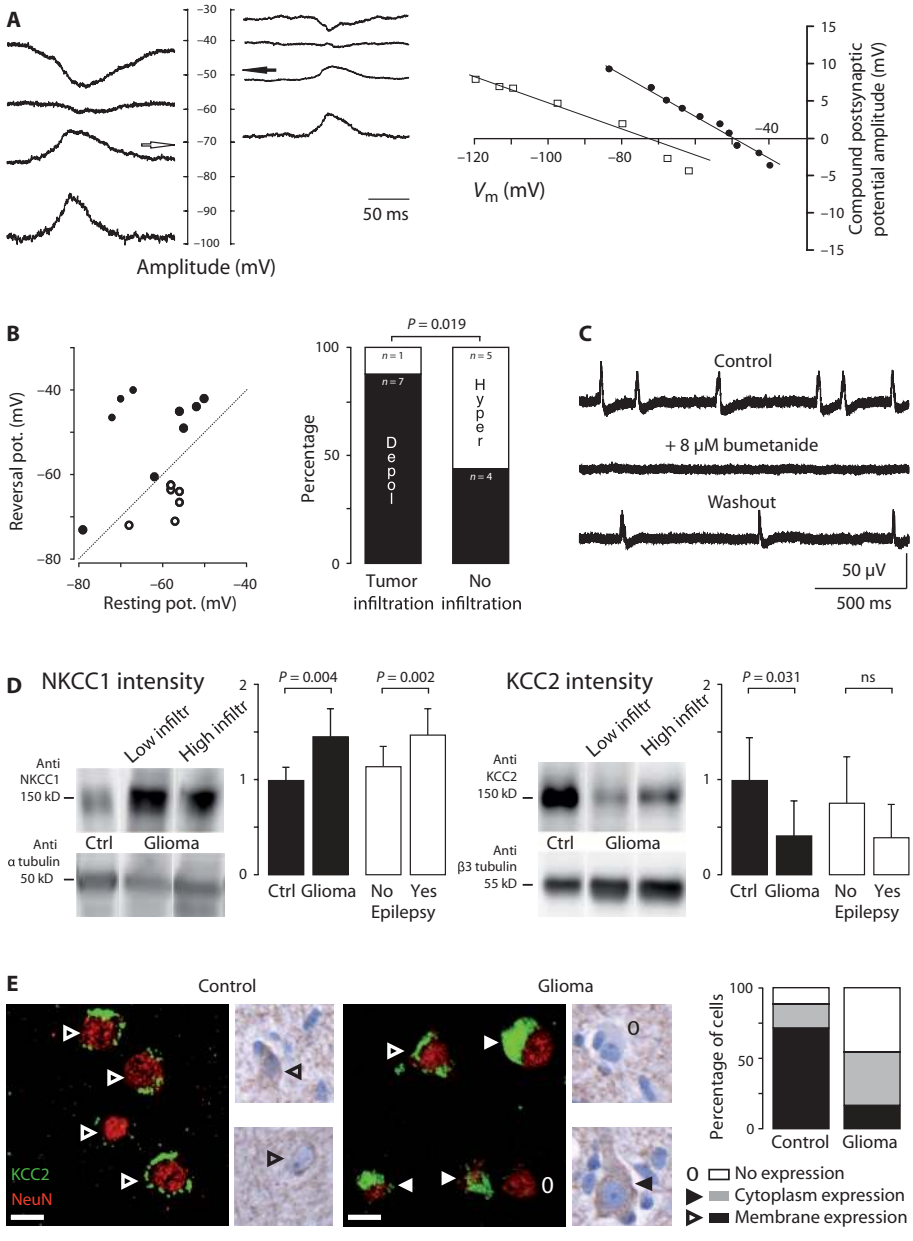

Fig. 4. Cl^- regulation impairment contributes to IIDs. (**A**) $GABA_A$ reversal potential (V_{rev}) in pyramidal cells. PSP amplitude during IIDs was measured in pyramidal cells of the neocortex infiltrated by glioma cells maintained at different potentials. Records are shown (at the left) and membrane potential (V_m) plotted (at right) from one cell with a V_{rev} of −71 mV (white arrow and open squares) and another cell with V_{rev} values of −48 mV (black arrow and filled circles). (**B**) Correlation of V_{rev} and resting potential for 15 pyramidal cells. Reversal potentials were depolarizing with respect to rest in nine cells (filled circles above the diagonal line), and hyperpolarizing in six cells (open circles below the line). The proportion of pyramidal cells depolarized by GABA during IIDs (black part of the histogram, "Depol" versus white part, "Hyper") was significantly higher in tissues with tumor infiltration than in tissues with no infiltration ($n = 17$ cells; $P = 0.019$, Fisher's exact test). (**C**) Blocking the K-Cl cotransporter NKCC1 with bumetanide (8 µM) reversibly suppressed spontaneous IID FPs. (**D**) Representative Western blots for NKCC1 (left) and KCC2 (right) in control neocortex and areas of low ("low infiltr") and high infiltration ("high infiltr") around human gliomas. NKCC1 expression was normalized to a nonneuronal-specific marker, α-tubulin. KCC2 expression was normalized to a neuron-specific marker, β3 tubulin. Histogram representing normalized NKCC1 protein quantification shows that NKCC1 is significantly increased in glioma samples as compared to controls ($n = 27$, $P = 0.004$, Mann-Whitney test) and in epileptic samples as compared to nonepileptic samples ($n = 27$, $P = 0.002$, Mann-Whitney test). Histogram representing normalized KCC2 protein quantification shows that KCC2 is significantly decreased in glioma samples as compared to controls ($n = 27$, $P = 0.031$, Mann-Whitney test) but not in epileptic samples as compared to nonepileptic samples ($n = 27$, $P = 0.158$, Mann-Whitney test). (**E**) Representative images of KCC2 immunoreactivity stained with neuronal nuclear antigen (NeuN) marker. Left: The fluorescence and the immunohistochemical labeling are distributed along the plasma membrane (arrowhead) of the cells in control tissue. Middle: In a glioma sample, the distribution of KCC2 immunoreactivity (fluorescence and immunohistochemistry) in neurons of infiltrated neocortex ranges from membrane staining (open arrowhead) to staining in the cytoplasmic region (filled arrowhead) to a loss of staining (open circle). Right: The quantification of KCC2 fluorescence redistribution for each cell shows a significant decrease of membrane staining ($n = 27$, $P = 0.01$, Fisher's exact test) and a significant increase in the loss of staining ($n = 27$, $P = 0.04$, Fisher's exact test) in glioma samples as compared to controls. Scale bar, 10 µm.

(45 ± 13.2%) than in control tissue (12 ± 6.5%) ($P = 0.04$). Furthermore, when KCC2 was detected in neurons of peritumoral neocortex, immunostaining tended to be cytoplasmic (38.6%) rather than membranous (15.8%), compared to a largely membranous (71.3%) rather than cytoplasmic (16.2%) expression in control neurons. Exclusive membrane KCC2 immunostaining was much lower in neurons of peritumoral neocortex (15.8 ± 6.7%) than controls (71.3 ± 4.2%) ($P = 0.01$). These differences in neuronal expression site should reduce KCC2 functionality in peritumoral neurons.

Together, these data point to an impaired Cl^- homeostasis in epileptogenic neocortex surrounding a glioma. GABA-mediated depolarization of a majority of peritumoral pyramidal cells is correlated with both an increase of NKCC1 expression and a loss of KCC2 immunoreactivity.

Induction of ictal-like activity

Ictal-like discharges (IDs) were induced pharmacologically in peritumoral tissue. Combining two proconvulsant stimuli, an increase of extracellular K^+ to 8 mM and a reduction of external Mg^{2+} to 0.25 mM (*24*), induced IDs in 7 of 19 slices (36.8%) where IIDs were generated (3 of 8 patients, 37.5%). Two ID patterns could be distinguished (Fig. 5A). The first consisted of recurrent rhythmic bursts of frequency 2.9 ± 0.9 Hz

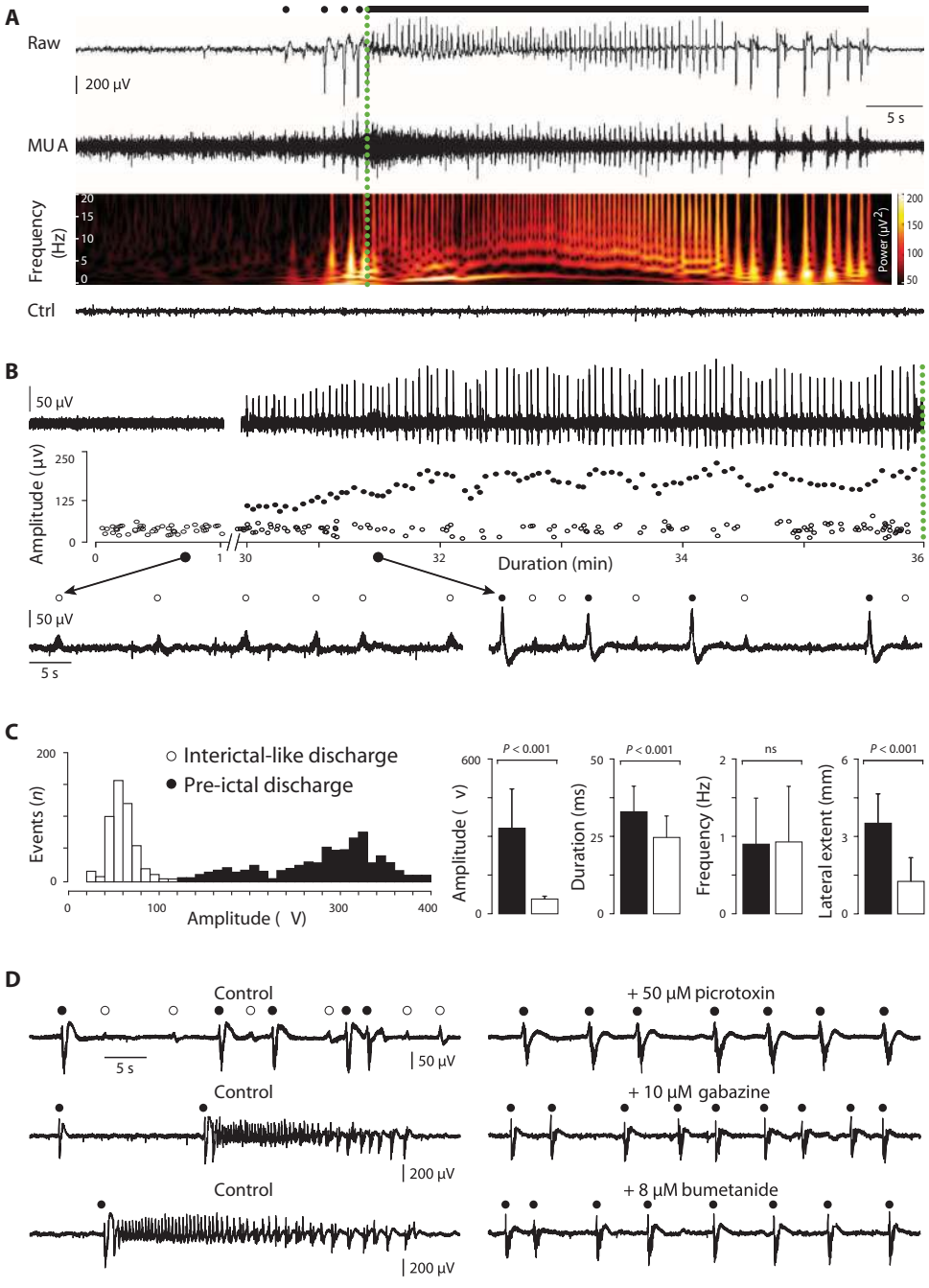

Fig. 5. IDs are preceded by a specific preictal activity. (**A**) Extracellular records of an ID induced by exposure to 0.25 mM Mg^{2+} and 8 mM K^+ in the infiltrated neocortex. PIDs (black-filled circles) recurred before seizure onset, followed by rhythmic bursts. MUA and time frequency plot of the local field potential are shown below. The green dotted line shows the onset of the seizure-like event. Ctrl shows a record from noninfiltrated neocortex in a control tissue from another tumor specimen with only an individual cell firing and no IID, PID, or ID after exposure to 0.25 mM Mg^{2+} and 8 mM K^+ for 90 min. (**B**) PIDs emerge during the transition to ictal-like activity in vitro. Extracellular records of the transition to ictal-like activity (0.25 mM Mg^{2+} and 8 mM K^+). The green dotted line shows the onset of the seizure-like event. Amplitudes of FPs during the transition show the emergence of larger PIDs (filled circles), but the amplitudes of IIDs (open circles) did not change. Bottom: IIDs before convulsant application (left) and co-occurrence of PIDs and IIDs during the transition (right). (**C**) Differences in IID and PID FPs. Amplitude distributions of all FPs during the transition distinguish between IIDs and PIDs. Mean ± SD of the amplitude ($n = 913$ events, $P < 0.001$, Mann-Whitney test), duration ($n = 913$ events, $P < 0.001$, Mann-Whitney test), frequency ($n = 913$ events, $P = 0.193$, Mann-Whitney test), and lateral extent ($n = 913$ events, $P < 0.001$, Mann-Whitney test) of IIDs (white) and PIDs (black) at steady state. (**D**) PIDs do not depend on GABAergic signaling. Extracellular records of IIDs (white dots), PIDs (black dots), and IDs at steady state in a 0.25 mM Mg^{2+} and 8 mM K^+ solution. The $GABA_A$ receptor antagonist picrotoxin (50 µM, for 30 min) reversibly blocked IIDs, but not PIDs (upper trace). The $GABA_A$ receptor antagonist gabazine (10 µM, for 40 min) blocked IDs, but not PIDs (middle trace). The NKCC1 antagonist bumetanide (8 µM, for 45 min) blocked IDs, but not PIDs (lower trace).

(range, 1.2 to 4.3; $n = 34$ events). The second involved an initial fast, low-voltage activity (mean duration, 0.8 ± 0.1 s; range, 0.65 to 0.99; $n = 8$ events) at 270 ± 97 Hz (range, 118 to 410), which then evolved into rhythmic bursts. The mean duration of IDs was 34.1 ± 17.7 s (range, 6.2 to 62.1). The transition from IIDs to IDs occurred over 34.0 ± 10.2 min (range, 20 to 50; $n = 6$ slices). IDs then recurred at an interval of 54.7 ± 62.4 s (range, 7.5 to 397.0; $n = 86$ events) in the continued presence of proconvulsants. Slices of control brain tissue ($n = 14$) did not generate IDs in response to the same proepileptic stimuli, increasing extracellular K^+ to 8 mM alone ($n = 8$ slices) or coupled to a reduction of external Mg^{2+} to 0.25 mM ($n = 6$ slices) (Fig. 5A).

Pre-ictal discharge emergence and dynamics

Pre-ictal discharges (PIDs) were recorded in 14 of 19 slices exposed to proconvulsant stimuli. In 7 of 7 slices, PIDs preceded IDs, and comparable large field potentials were detected in 7 of 12 slices that did not exhibit later IDs. PID amplitude increased during the transition to ictal discharges, and PIDs occurred concurrently with IIDs during this transition (Fig. 5, B and C). At steady state ($n = 446$ events from 5 slices), PID amplitude and duration were larger than those of IIDs (mean, 336 ± 114 versus 58 ± 11 μV, $P < 0.001$, $n = 446$; 32.5 ± 8.6 versus 24.4 ± 7.9 ms, $n = 446$ and 467 events, $P < 0.0001$), but frequencies were similar (0.9 ± 0.6 versus 0.93 ± 0.7 Hz; $P = 0.727$). PID fields were recorded from column-like regions with maximal amplitude in superficial neocortical layers III and IV (7 of 7 slices) at distances of 1.4 ± 0.7 mm (range, 1 to 3; $n = 7$ slices) from the pia mater. PIDs propagated laterally for distances up to 3.5 ± 1.3 mm (range, 1.5 to 5; $n = 9$ slices) from their initiation site. PIDs were never induced by identical stimuli in slices of control tissue ($n = 14$).

We next examined the role of GABAergic signaling in PIDs and IDs and compared it to the pharmacology of IIDs. PIDs were not affected by $GABA_A$ receptor antagonists (picrotoxin, 50 μM; $n = 4$; gabazine, 10 μM; $n = 3$ patients; application of 45 to 70 min; Fig. 5D). Both IIDs and IDs were reversibly suppressed by the same $GABA_A$ receptor antagonists (picrotoxin, 50 μM; $n = 4$; gabazine, 10 μM; $n = 3$ patients) over a mean period of 33 ± 6.6 min (range, 30 to 40; Fig. 5D). This pharmacological profile suggests the involvement of depolarizing effects of GABA on IIDs and IDs. We therefore tested the effects of the blockade of the Cl^- cotransporter NKCC1 with low doses of the diuretic bumetanide. At 8 μM, bumetanide abolished IIDs and IDs within 45 min ($n = 4$) (Fig. 5D). As expected, it did not affect PIDs in records longer than 75 min (Fig. 5D).

HFOs associated with PIDs differed from those nested in IIDs (Fig. 6A). HFOs were detected in 91% of electrodes recording PIDs (11 of 12; $n = 3$ patients) as opposed to ~40% for IIDs. HFOs occurred

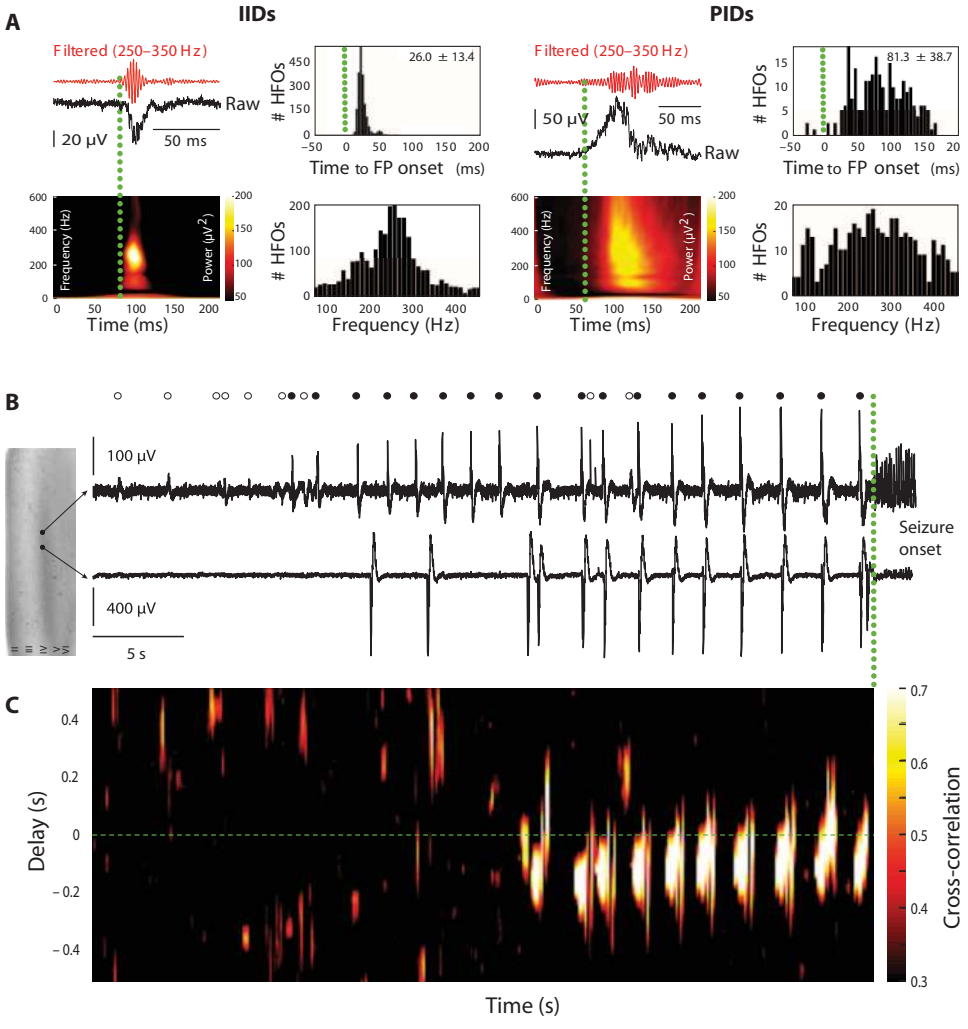

Fig. 6. Interictal, pre-ictal, and onset of ictal-like events depend on dynamic organization of population activities. and onset of ictal-like events depend on dynamic organization of population activities. (**A**) HFOs occurring during IIDs (left, $n = 284$ events) and PIDs (right, $n = 294$ events). For each type of activity, top left: HFO recording (red trace) during an FP (black trace); bottom left: HFO time frequency representation; top right: histogram of HFO timing with respect to a population event (the mean frequency ± SD is indicated); bottom right: histogram of HFO frequency distribution during population event. Population FP onset is shown as a green dotted line. Mean frequency of HFOs during IIDs and PIDs was 266 ± 90 Hz versus 251 ± 69 Hz, respectively. HFOs associated with IIDs had a narrow frequency spectrum and were restricted to the onset of an IID. HFOs during PIDs spanned the frequency spectrum and persisted throughout PIDs. (**B**) Dual extracellular records during the initiation of a seizure-like event, with seizure onset shown by a green dotted line. IIDs (open circles) and PIDs (filled circles) during the transition are shown above. PIDs are progressively recruited and recur before seizure onset. (**C**) Time delay and cross correlation of PIDs initiated at two distinct foci recorded by two electrodes. During seizure initiation, synchrony progressively increased, and propagation delay between the two PID foci was reduced.

throughout PIDs but were restricted to IID onset. The range of HFO frequencies associated with PIDs was wider than that for IIDs, although mean dominant frequencies were similar (266 ± 90 versus 251 ± 69 Hz). These data suggest that IIDs and PIDs may result from distinct processes with different spatial and temporal characteristics.

We explored the dynamics of PIDs at ID onset. Once IDs occurred in recurring fashion, each ID (n = 34 events; n = 7 slices) was preceded by 5 ± 4 PIDs (range, 1 to19) during 11.7 ± 7.7 s (range, 3.5 to 36.9) at a frequency of 0.46 ± 0.2 Hz (range, 0.07 to 0.69). When PIDs were generated at distinct foci, the transition to ID was associated with an increased synchrony and conduction speed between foci (n = 12 events from 2 slices from 2 patients) (Fig. 6, B and C).

These data indicate that the neocortex surrounding glioma generates two forms of synchronous epileptiform activities during the transition to IDs. IIDs depend on depolarizing GABA and AMPA receptor–mediated glutamatergic signaling, whereas GABAergic transmission does not contribute to PIDs. ID initiation requires functional GABAergic signaling and involves depolarizing effects of GABA, which could be related to Cl^- accumulation in pyramidal cells, induced by recurring, synchronous PIDs.

DISCUSSION

We have shown that peritumoral neocortex infiltrated by glioma cells in slices of human tissue generates spontaneous epileptic discharges, which depend on both AMPA glutamatergic and GABAergic signaling. The onset of IIDs was preceded by interneuron firing. GABA depolarized a small majority of pyramidal cells in infiltrated tissues, reflecting changes in Cl^- homeostasis due to both a reduced KCC2 and increased NKCC1 expression. Excited peritumoral tissue generated IDs preceded by PIDs, but none of these glioma-related epileptiform activities were detected in nonepileptic control tissue. Features of epileptiform activities generated by peritumoral cortex were similar to those of nontumoral, sclerotic, epileptic human temporal lobe (*21*, *22*, *24*), suggesting a common basis of pathological activities.

This spontaneous population synchrony generated by tissue from adult patients with gliomas should be classified as epileptic because (i) it is comparable to interictal epileptic activity recorded during glioma surgery (*3*–*5*); (ii) neuronal activity was recorded from most slices, but only half of the tissues generated IIDs; (iii) IIDs were generated focally at similar sites in adjacent slices from the same brain tissue; (iv) IIDs were generated in multiple peritumoral foci (*4*, *5*), but never in control samples; (v) HFOs, linked to zones of active epileptogenesis (*39*, *40*), were nested in IIDs; and (vi) IDs were induced exclusively in slices that generated IIDs. Thus, the peritumoral neocortex around gliomas is a pivotal structure both for the genesis of epileptic activity and for infiltration by glioma cells (*6*, *7*). This link may explain the antiepileptic effects of oncologic treatments (*41*–*44*) and the increase in seizure frequency as tumors progress (*45*).

Our data suggest that interneuron firing preceded IIDs. The resulting pyramidal cell depolarization may contribute to IID initiation because $GABA_A$ receptor activation depolarized ~60% of pyramidal cells of peritumoral neocortex, owing to an excessive Cl^- load mediated by NKCC1. These data recall results from sclerotic nontumoral human epileptic tissue (*21*, *22*) and are consistent with molecular defects identified in peritumoral tissues (*32*). In neurons with altered Cl^- homeostasis, the reversal potential of GABA-evoked current depolarizes, and the efficacy of GABAergic inhibition is reduced (*32*). Reversal potentials measured here, based on compound GABAergic and glutamatergic PSPs, point to depolarizing effects of GABA. Our results support disequilibrium between an excitatory glutamatergic drive and an inhibitory GABAergic brake, a brake that can be switched into an accelerator. An increased glutamatergic drive (*8*, *14*, *16*, *17*), due to both an increased release from glioma cells via the system x_c^- cystine-glutamate transporter (*9*, *12*) and impaired glutamate uptake by glial cells (*11*), would contribute to synchrony and excitotoxicity (*8*, *12*). Conversely, perturbed GABAergic signaling in peritumoral tissue may favor oncogenesis, and it is known that GABA regulates glioma cell proliferation (*29*). Intracellular Cl^- concentrations in migrating and proliferating glioma cells may reach ~100 mM (*26*, *27*). These concentrations are actively maintained by the NKCC1 cotransporter (*26*, *31*), which is strongly expressed in glioma cells (*30*, *32*) and gangliogliomas (human glioneuronal tumors) (*32*, *46*). Blockade of NKCC1 reduces tumor growth in animal models (*31*). Several mechanisms may contribute to NKCC1 up-regulation in peritumoral neurons: (i) extracellular hyperosmolarity (*47*) due to Cl^- and K^+ release by tumor cells may enhance neuronal NKCC1 expression (*27*, *48*); (ii) BDNF (brain-derived neurotrophic factor) release by glioma cells (*49*, *50*) reduces KCC2 expression (*51*) and so should weaken Cl^- extrusion; (iii) the activation of WNK kinases by epidermal growth factor receptor–dependent signals may activate NKCC1 in both glioma cells and neurons (*52*); (iv) newly formed neurons emerging from neurogenesis in response to glioma development may share an immature phenotype (*53*). We note that NKCC1 expression does not depend on tumor grade and that more neurons were depolarized by GABA in grade IV gliomas, although they are less often associated with seizures than low-grade gliomas (*54*, *55*). This apparent paradox may be explained if highly destructive and rapidly growing grade IV gliomas restrain epileptogenicity.

This study, performed on human tissue rather than animal models of gliomas, has some limitations. Synaptic connectivity is reduced in slices, and influences from distant brain regions are lost. The slicing procedure traumatizes and may alter Cl^- regulation in neurons at depths less than 50 μm from the surface (*56*). However, most cells in this study were recorded deeper, no abnormal activity was obtained from control tissues, and epileptiform activities were reliably produced by the same area in adjacent slices. Furthermore, in an animal model of brain tumors, the seizure threshold assessed by $GABA_A$ blocker administration was increased compared to controls (*57*), suggesting that our results have in vivo correlates. In some areas, abnormal or epileptiform activities were recorded in slices, but seizures were not detected preoperatively, possibly because in situ, these aberrant electrical events remained restricted and did not reach a threshold for propagation. Seizures might also be missed or delayed in patients with gliomas.

Altogether, these data point to a similar defect in Cl^- homeostasis and GABAergic signaling in two distinct epileptic syndromes: peritumoral cortical regions of human gliomas and sclerotic human temporal lobe (*21*, *22*, *24*). This defect, together with an excessive glutamatergic excitatory drive, may be a common feature of human epileptogenesis. Further, molecules that control Cl^- homeostasis may be useful therapeutic targets for both epileptogenesis, as highlighted in the present study, and tumor infiltration, as previously studied in animal models (*31*). The efficacy of GABAergic antiepileptic drugs and their potential negative effects on glioma evolution will need to be investigated.

SUPPLEMENTARY MATERIALS

www.sciencetranslationalmedicine.org/cgi/content/full/6/244/244ra89/DC1
Materials and Methods
Fig. S1. $CD3^+$, $CD20^+$, $CD68^+$, and $Ki67^+$ cells do not influence IIDs in regions of tumor infiltration.
Fig. S2. NKCC1 expression does not depend on tumor infiltration or tumor grade in glioma-infiltrated neocortex.
Table S1. Clinical, imaging, neuropathological, molecular, and follow-up findings of the 47 patients under study.
References (*58*–*60*)

REFERENCES AND NOTES

1. M.S. van Breemen, E. B. Wilms, C. J. Vecht, Epilepsy in patients with brain tumours: Epidemiology, mechanisms, and management. *Lancet Neurol.* **6**, 421–430 (2007).
2. J. Pallud, L. Capelle, G. Huberfeld, Tumoral epileptogenicity: How does it happen? *Epilepsia* **54**, 30–34 (2013).
3. J. F. Hirsch, J. Buisson-Ferey, M. Sachs, J. C. Hirsch, J. Scherrer, Electrocorticogram and unitary activites with expanding lesions in man. *Electroencephalogr. Clin. Neurophysiol.* **21**, 417–428 (1966).
4. M. S. Berger, S. Ghatan, M. M. Haglund, J. Dobbins, G. A. Ojemann, Low-grade gliomas associated with intractable epilepsy: Seizure outcome utilizing electrocorticography during tumor resection. *J. Neurosurg.* **79**, 62–69 (1993).
5. M. M. Haglund, M. S. Berger, D. D. Kunkel, J. E. Franck, S. Ghatan, G. A. Ojemann, Changes in γ-aminobutyric acid and somatostatin in epileptic cortex associated with low-grade gliomas. *J. Neurosurg.* **77**, 209–216 (1992).
6. J. Pallud, P. Varlet, B. Devaux, S. Geha, M. Badoual, C. Deroulers, P. Page, E. Dezamis, C. Daumas-Duport, F. X. Roux, Diffuse low-grade oligodendrogliomas extend beyond MRI-defined abnormalities. *Neurology* **74**, 1724–1731 (2010).
7. J. Pallud, Diffuse low-grade gliomas: What does "complete resection" mean? in *Tumors of the central nervous system: Gliomas, glioblastomas. Part 2.* (Springer Netherlands, Dordrecht, 2011), pp. 153–161.
8. S. C. Buckingham, S. L. Campbell, B. R. Haas, V. Montana, S. Robel, T. Ogunrinu, H. Sontheimer, Glutamate release by primary brain tumors induces epileptic activity. *Nat. Med.* **17**, 1269–1274 (2011).
9. A. Bordey, H. Sontheimer, Electrophysiological properties of human astrocytic tumor cells in situ: Enigma of spiking glial cells. *J. Neurophysiol.* **79**, 2782–2793 (1998).
10. M. L. Olsen, H. Sontheimer, Functional implications for Kir4.1 channels in glial biology: From K^+ buffering to cell differentiation. *J. Neurochem.* **107**, 589–601 (2008).
11. Z. C. Ye, J. D. Rothstein, H. Sontheimer, Compromised glutamate transport in human glioma cells: Reduction–mislocalization of sodium-dependent glutamate transporters and enhanced activity of cystine–glutamate exchange. *J. Neurosci.* **19**, 10767–10777 (1999).
12. J. de Groot, H. Sontheimer, Glutamate and the biology of gliomas. *Glia* **59**, 1181–1189 (2011).
13. T. Takano, J. H. Lin, G. Arcuino, Q. Gao, J. Yang, M. Nedergaard, Glutamate release promotes growth of malignant gliomas. *Nat. Med.* **7**, 1010–1015 (2001).
14. A. Hamberger, B. Nyström, S. Larsson, H. Silfvenius, C. Nordborg, Amino acids in the neuronal microenvironment of focal human epileptic lesions. *Epilepsy Res.* **9**, 32–43 (1991).
15. S. A. Lyons, W. J. Chung, A. K. Weaver, T. Ogunrinu, H. Sontheimer, Autocrine glutamate signaling promotes glioma cell invasion. *Cancer Res.* **67**, 9463–9471 (2007).
16. H. J. Marcus, K. L. Carpenter, S. J. Price, P. J. Hutchinson, In vivo assessment of high-grade glioma biochemistry using microdialysis: A study of energy-related molecules, growth factors and cytokines. *J. Neurooncol.* **97**, 11–23 (2010).
17. M. Roslin, R. Henriksson, P. Bergström, U. Ungerstedt, A. T. Bergenheim, Baseline levels of glucose metabolites, glutamate and glycerol in malignant glioma assessed by stereotactic microdialysis. *J. Neurooncol.* **61**, 151–160 (2003).
18. H. K. Wolf, D. Roos, I. Blümcke, T. Pietsch, O. D. Wiestler, Perilesional neurochemical changes in focal epilepsies. *Acta Neuropathol.* **91**, 376–384 (1996).
19. P. Marco, R. G. Sola, S. Ramón y Cajal, J. DeFelipe, Loss of inhibitory synapses on the soma and axon initial segment of pyramidal cells in human epileptic peritumoural neocortex: Implications for epilepsy. *Brain Res. Bull.* **44**, 47–66 (1997).
20. B. Schaller, S. J. Rüegg, Brain tumor and seizures: Pathophysiology and its implications for treatment revisited. *Epilepsia* **44**, 1223–1232 (2003).
21. I. Cohen, V. Navarro, S. Clemenceau, M. Baulac, R. Miles, On the origin of interictal activity in human temporal lobe epilepsy in vitro. *Science* **298**, 1418–1421 (2002).
22. G. Huberfeld, L. Wittner, S. Clemenceau, M. Baulac, K. Kaila, R. Miles, C. Rivera, Perturbed chloride homeostasis and GABAergic signaling in human temporal lobe epilepsy. *J. Neurosci.* **27**, 9866–9873 (2007).
23. R. Köhling, A. Lücke, H. Straub, E. J. Speckmann, I. Tuxhorn, P. Wolf, H. Pannek, F. Oppel, Spontaneous sharp waves in human neocortical slices excised from epileptic patients. *Brain* **121** (Pt. 6), 1073–1087 (1998).
24. G. Huberfeld, L. Menendez de la Prida, J. Pallud, I. Cohen, M. Le Van Quyen, C. Adam, S. Clemenceau, M. Baulac, R. Miles, Glutamatergic pre-ictal discharges emerge at the transition to seizure in human epilepsy. *Nat. Neurosci.* **14**, 627–634 (2011).
25. R. Miles, P. Blaesse, G. Huberfeld, L. Wittner, K. Kaila, in *Chloride Homeostasis and GABA Signaling in Temporal Lobe Epilepsy*, J. L. Noebels, M. Avoli, M. A. Rogawski, R. W. Olsen, A. V. Delgado-Escueta, Eds. [National Center for Biotechnology Information (US), Bethesda (MD), ed. 4, 2012].
26. C. W. Habela, N. J. Ernest, A. F. Swindall, H. Sontheimer, Chloride accumulation drives volume dynamics underlying cell proliferation and migration. *J. Neurophysiol.* **101**, 750–757 (2009).
27. C. W. Habela, M. L. Olsen, H. Sontheimer, ClC3 is a critical regulator of the cell cycle in normal and malignant glial cells. *J. Neurosci.* **28**, 9205–9217 (2008).
28. C. Labrakakis, S. Patt, J. Hartmann, H. Kettenmann, Functional $GABA_A$ receptors on human glioma cells. *Eur. J. Neurosci.* **10**, 231–238 (1998).
29. S. Z. Young, A. Bordey, GABA's control of stem and cancer cell proliferation in adult neural and peripheral niches. *Physiology (Bethesda)* **24**, 171–185 (2009).
30. N. J. Ernest, H. Sontheimer, Extracellular glutamine is a critical modulator for regulatory volume increase in human glioma cells. *Brain Res.* **1144**, 231–238 (2007).
31. B. R. Haas, H. Sontheimer, Inhibition of the Sodium-Potassium-Chloride Cotransporter Isoform-1 reduces glioma invasion. *Cancer Res.* **70**, 5597–5606 (2010).
32. L. Conti, E. Palma, C. Roseti, C. Lauro, R. Cipriani, M. de Groot, E. Aronica, C. Limatola, Anomalous levels of Cl^- transporters cause a decrease of GABAergic inhibition in human peritumoral epileptic cortex. *Epilepsia* **52**, 1635–1644 (2011).
33. D. N. Louis, H. Ohgaki, O.D. Wiestler, W. K. Cavenee (Eds.), World Health Organization Classification of Tumours of the Central Nervous System (IARC press, 2007).
34. A. Bragin, I. Mody, C. L. Wilson, J. Engel Jr., Local generation of fast ripples in epileptic brain. *J. Neurosci.* **22**, 2012–2021 (2002).
35. L. Menendez de la Prida, R. Benavides-Piccione, R. Sola, M. A. Pozo, Electrophysiological properties of interneurons from intraoperative spiking areas of epileptic human temporal neocortex. *Neuroreport* **13**, 1421–1425 (2002).
36. V. I. Dzhala, D. M. Talos, D. A. Sdrulla, A. C. Brumback, G. C. Mathews, T. A. Benke, E. Delpire, F. E. Jensen, K. J. Staley, NKCC1 transporter facilitates seizures in the developing brain. *Nat. Med.* **11**, 1205–1213 (2005).
37. C. Rivera, J. Voipio, J. A. Payne, E. Ruusuvuori, H. Lahtinen, K. Lamsa, U. Pirvola, M. Saarma, K. Kaila, The K^+/Cl^- co-transporter KCC2 renders GABA hyperpolarizing during neuronal maturation. *Nature* **397**, 251–255 (1999).
38. N. J. Ernest, A. K. Weaver, L. B. Van Duyn, H. W. Sontheimer, Relative contribution of chloride channels and transporters to regulatory volume decrease in human glioma cells. *Am. J. Physiol. Cell Physiol.* **288**, C1451–C1460 (2005).
39. J. Engel Jr., A. Bragin, R. Staba, I. Mody, High-frequency oscillations: What is normal and what is not? *Epilepsia* **50**, 598–604 (2009).
40. G. Foffani, Y. G. Uzcategui, B. Gal, L. Menendez de la Prida, Reduced spike-timing reliability correlates with the emergence of fast ripples in the rat epileptic hippocampus. *Neuron* **55**, 930–941 (2007).
41. M. M. Zaatreh, K. S. Firlik, D. D. Spencer, S. S. Spencer, Temporal lobe tumoral epilepsy: Characteristics and predictors of surgical outcome. *Neurology* **61**, 636–641 (2003).
42. R. Soffietti, B. G. Baumert, L. Bello, A. von Deimling, H. Duffau, M. Frénay, W. Grisold, R. Grant, F. Graus, K. Hoang-Xuan, M. Klein, B. Melin, J. Rees, T. Siegal, A. Smits, R. Stupp, W. Wick, European Federation of Neurological Societies, Guidelines on management of low-grade gliomas: Report of an EFNS–EANO Task Force. *Eur. J. Neurol.* **17**, 1124–1133 (2010).
43. A. Pace, A. Vidiri, E. Galiè, M. Carosi, S. Telera, A. M. Cianciulli, P. Canalini, D. Giannarelli, B. Jandolo, C. M. Carapella, Temozolomide chemotherapy for progressive low-grade glioma: Clinical benefits and radiological response. *Ann. Oncol.* **14**, 1722–1726 (2003).
44. J. H. Sherman, K. Moldovan, H. K. Yeoh, R. M. Starke, N. Pouratian, M. E. Shaffrey, D. Schiff, Impact of temozolomide chemotherapy on seizure frequency in patients with low-grade gliomas. *J. Neurosurg.* **114**, 1617–1621 (2011).
45. A. Rosati, A. Tomassini, B. Pollo, C. Ambrosi, A. Schwarz, A. Padovani, B. Bonetti, Epilepsy in cerebral glioma: Timing of appearance and histological correlations. *J. Neurooncol.* **93**, 395–400 (2009).
46. E. Aronica, K. Boer, S. Redeker, W. G. Spliet, P. C. van Rijen, D. Troost, J. A. Gorter, Differential expression patterns of chloride transporters, Na^+-K^+-$2Cl^-$-cotransporter and K^+-Cl^--cotransporter, in epilepsy-associated malformations of cortical development. *Neuroscience* **145**, 185–196 (2007).
47. J. S. Kim, W. B. Kim, Y. B. Kim, Y. Lee, Y. S. Kim, F. Y. Shen, S. W. Lee, D. Park, H. J. Choi, J. Hur, J. J. Park, H. C. Han, C. S. Colwell, Y. W. Cho, Y. I. Kim, Chronic hyperosmotic stress converts GABAergic inhibition into excitation in vasopressin and oxytocin neurons in the rat. *J. Neurosci.* **31**, 13312–13322 (2011).
48. S. C. Buckingham, S. Robel, Glutamate and tumor-associated epilepsy: Glial cell dysfunction in the peritumoral environment. *Neurochem. Int.* **63**, 696–701 (2013).
49. Q. Yan, H. L. Yu, J. T. Li, Study on the expression of BDNF in human gliomas. *Sichuan Da Xue Xue Bao Yi Xue Ban* **40**, 415–417 (2009).

50. A. Chiaretti, L. Aloe, A. Antonelli, A. Ruggiero, M. Piastra, R. Riccardi, G. Tamburrini, C. Di Rocco, Neurotrophic factor expression in childhood low-grade astrocytomas and ependymomas. *Childs Nerv. Syst.* **20**, 412–419 (2004).
51. C. Rivera, J. Voipio, J. Thomas-Crusells, H. Li, Z. Emri, S. Sipilä, J. A. Payne, L. Minichiello, M. Saarma, K. Kaila, Mechanism of activity-dependent downregulation of the neuron-specific K-Cl cotransporter KCC2. *J. Neurosci.* **24**, 4683–4691 (2004).
52. K. T. Kahle, J. Rinehart, P. de Los Heros, A. Louvi, P. Meade, N. Vazquez, S. C. Hebert, G. Gamba, I. Gimenez, R. P. Lifton, WNK3 modulates transport of Cl^- in and out of cells: Implications for control of cell volume and neuronal excitability. *Proc. Natl. Acad. Sci. U.S.A.* **102**, 16783–16788 (2005).
53. J. Macas, M. C. Ku, C. Nern, Y. Xu, H. Bühler, M. Remke, M. Synowitz, K. Franz, V. Seifert, K. H. Plate, H. Kettenmann, R. Glass, S. Momma, Generation of neuronal progenitor cells in response to tumors in the human brain. *Stem Cells* **32**, 244–257 (2014).
54. K. Lote, A. E. Stenwig, K. Skullerud, H. Hirschberg, Prevalence and prognostic significance of epilepsy in patients with gliomas. *Eur. J. Cancer* **34**, 98–102 (1998).
55. J. Pallud, E. Audureau, M. Blonski, N. Sanai, L. Bauchet, D. Fontaine, E. Mandonnet, E. Dezamis, D. Psimaras, J. Guyotat, P. Peruzzi, P. Page, B. Gal, E. Párraga, M. H. Baron, M. Vlaicu, R. Guillevin, B. Devaux, H. Duffau, L. Taillandier, L. Capelle, G. Huberfeld, Epileptic seizures in diffuse low-grade gliomas in adults. *Brain* **137**, 449–462 (2014).
56. V. Dzhala, G. Valeeva, J. Glykys, R. Khazipov, K. Staley, Traumatic alterations in GABA signaling disrupt hippocampal network activity in the developing brain. *J. Neurosci.* **32**, 4017–4031 (2012).
57. A. Beaumont, M. Clarke, I. R. Whittle, The effects of malignant glioma on the EEG and seizure thresholds: An experimental study. *Acta Neurochir.* **138**, 370–381 (1996).
58. S. E. Connor, R. Gunny, T. Hampton, R. O'gorman, Magnetic resonance image registration and subtraction in the assessment of minor changes in low grade glioma volume. *Eur. Radiol.* **14**, 2061–2066 (2004).
59. M. A. Hammoud, B. L. Ligon, R. elSouki, W. M. Shi, D. F. Schomer, R. Sawaya, Use of intra-operative ultrasound for localizing tumors and determining the extent of resection: A comparative study with magnetic resonance imaging. *J. Neurosurg.* **84**, 737–741 (1996).
60. R. J. Staba, C. L. Wilson, A. Bragin, I. Fried, J. Engel Jr., Quantitative analysis of high-frequency oscillations (80–500 Hz) recorded in human epileptic hippocampus and entorhinal cortex. *J. Neurophysiol.* **88**, 1743–1752 (2002).

Acknowledgments: We thank L. Menendez de la Prida, S. Mahon, and S. Charpier for critical reading of the manuscript. We are grateful to K. Mokthari, C. Adam, and to the staff of the Service de Neuropathologie for the excellent technical assistance. We thank C. Lytle (University of California, Riverside) and K. Kaila (University of Helsinki) for gifts of antibodies. We also thank C. Karachi, F. Chrétien, C. Oppenheim, J.-F. Meder, and E. Dezamis for their neurosurgical, neuroimaging, and neuropathological contributions. The paper is dedicated to Marceau who was born during the late revision process. **Funding:** Supported by grants from the UPMC (Convergence CVG1106), the INSERM, the CNRS, the AP-HP, the Fédération pour la Recherche sur le Cerveau, the European Research Council (322721). **Author contributions:** J.P., N.C., and G.H. performed experiments. M.L.V.Q., J.P., and G.H. analyzed electrophysiological data. F.B., C.P., P.V., N.K., M.-J.D., M.L., G.C. and C.D. performed morphological and immunohistochemical analyses. M.B., B.D., C.R., R.M., L.C., J.P., and G.H. contributed to the design of the experiments. L.C. and J.P. provided postoperative tissues. J.P. and G.H. wrote the manuscript. **Competing interests:** P.V. serves as a consultant on the advisory boards of Hoffmann-La Roche and Boehringer Ingelheim. The other authors declare that they have no competing interests.

Submitted 18 November 2013
Accepted 6 May 2014
Published 9 July 2014
10.1126/scitranslmed.3008065

Citation: J. Pallud, M. Le Van Quyen, F. Bielle, C. Pellegrino, P. Varlet, M. Labussiere, N. Cresto, M.-J. Dieme, M. Baulac, C. Duyckaerts, N. Kourdougli, G. Chazal, B. Devaux, C. Rivera, R. Miles, L. Capelle, G. Huberfeld, Cortical GABAergic excitation contributes to epileptic activities around human glioma. *Sci. Transl. Med.* **6**, 244ra89 (2014).